A Direct Sampling Method for Electrical Impedance Tomography

Yat Tin Chow* Kazufumi Ito† Jun Zou‡

Abstract

This work investigates the electrical impedance tomography (EIT) problem in the case when only one or two pairs of Cauchy data is available, which is known to be very difficult in achieving high reconstruction quality owing to its severely ill-posed nature. We propose a simple and efficient direct sampling method (DSM) to locate inhomogeneous inclusions. A new probing function based on the dipole potential is introduced to construct an indicator function for imaging the inclusions. Explicit formulae for the probing and indicator functions are derived in the case when the sampling domain is of spherical geometry in $\mathbb{R}^n$ $(n = 2, 3)$. This new method is easy to implement and computationally cheap. Numerical experiments are presented to demonstrate the robustness and effectiveness of the DSM, which provides a new numerical approach for solving the EIT problem.

Mathematics Subject Classification (MSC 2000): 35R30, 65F22, 65M32, 65N21, 86A22.

Keywords: electrical impedance tomography, limited data, inhomogeneous inclusions, probing function, indicator function, reconstruction algorithm

1 Introduction

Electrical impedance tomography (EIT) is an effective noninvasive evaluation method that creates images of the electrical conductivity of an inhomogeneous medium by applying currents at a number of electrodes on the boundary and measuring the corresponding voltages. The EIT problem was first considered as a mathematical problem by Calderón in 1980 [15], in which he considered the inverse problem of whether the electrical conductivity of a medium can be recovered by the boundary voltage and current measurements. A detailed survey of the mathematical studies on the EIT problem can be found in [55]. EIT has now found applications in many areas, such as oil and geophysical prospection [59], medical imaging [28], physiological measurement [29], early diagnosis of breast cancer [38, 60], monitoring of pulmonary functions [31] and detection of leaks from buried pipes [37], as well as many other applications [6, 24, 27, 53, 54]. Our application of EIT is the detection of some embedded inclusions in a known homogeneous background, e.g., one may think of air bubbles, cracks, defects or impurities in an otherwise homogeneous medium of building material or biological tissue.

It is known that the severe ill-posedness makes it more difficult to have high quality image reconstruction for the EIT problem than for many other imaging problems. Focus has therefore been put to develop efficient and stable numerical algorithms to achieve some reasonable EIT imaging, see, e.g., [5, 9, 18, 19, 21, 35, 41, 46, 51, 56, 58]. Some of the algorithms are based on the technique of minimization of a least-squares residual functional combined with a Tikhnov regularization. Various regularizers have been studied, such as Sobolev regularization [39, 46, 56], total variation regularization [19, 21, 51], and regularizations which incorporate a priori structural information [45]. Numerical analysis for EIT imaging techniques based on Tikhonov regularization can be found in [46, 50, 51]. The d-bar method is also proposed to solve the EIT problem [52]. Recently, the concept of sparsity and statistical inversion

*Department of Mathematics, The Chinese University of Hong Kong, Shatin, Hong Kong. (ytchow@math.cuhk.edu.hk).

†Department of Mathematics and Center for Research in Scientific Computation, North Carolina State University, Raleigh, North Carolina (kito@unity.ncsu.edu).

‡Department of Mathematics, Chinese University of Hong Kong, Shatin, N.T., Hong Kong. The work of this author was substantially supported by Hong Kong RGC grants (projects 405513 and 404611). (zou@math.cuhk.edu.hk).

approach were also applied to the EIT imaging [40]. We may refer to [41, 47] for L^1-type regularization and [19, 10] for TV-type regularization with sparsity. Thorough theoretical studies, algorithms and numerical experiments were presented in [23, 34, 36]. In the last decade, another family of reconstruction algorithms for solving the EIT problem which are non-iterative in nature starts to flourish [7], most of which can also be referred as the direct methods. They provide a good alternative to the minimization algorithms and linearization approximations. Usually these direct methods propose indicator functions which attains extreme values when the sampling point belongs to the support of the inhomogeneities. Some of these newly developed direct techniques are developed based on spectral analysis, for instance, the sampling and factorization methods [7, 13, 26, 42], and the MUSIC algorithms [1, 2, 20]. Other direct techniques which involve different philosophy include the point source method [30] and the topological sensitivity approach [2, 8]. Recent systematic reviews on both the regularized minimization algorithms and the direct methods are available in [7, 33].

Now we describe the isotropic EIT model of our interest. Suppose $\Omega \subset \mathbb{R}^n$ $(n = 2, 3)$ is an open bounded connected domain with a C^2-boundary, containing some conducting media. Assume that σ is a strictly positive L^∞ function, representing an isotropic conductivity in Ω. Let σ_0 be the conductivity of the homogeneous background medium. We shall often denote the support of $\sigma - \sigma_0$ as D, representing the inhomogeneous inclusions. Then the potential $u \in H^1(\Omega)$ in the isotropic conductivity model satisfies the following equation [9]

$$\begin{cases} \nabla \cdot (\sigma \nabla u) &= 0 \quad \text{in} \quad \Omega\,, \\ \sigma \dfrac{\partial u}{\partial \nu} &= g \quad \text{on} \quad \partial\Omega \end{cases} \tag{1.1}$$

where the Neumann boundary data $g \in H^{-1/2}(\partial\Omega)$ represents the current imposed on the boundary. We shall complement the system (1.1) by the following condition for the uniqueness of the solution

$$\int_{\partial\Omega} u\, ds = 0\,. \tag{1.2}$$

For a given conductivity σ, we denote by Λ_σ the Neumann-to-Dirichlet (NtD) operator $\Lambda_\sigma : H^{-1/2}(\partial\Omega) \to H^{1/2}(\partial\Omega)$ given by

$$\Lambda_\sigma g = u|_{\partial\Omega}\,. \tag{1.3}$$

Correspondingly, we shall write Λ_{σ_0} for the Neumann-to-Dirichlet operataor associated with the homogeneous medium. From now on, we will often write the surface potential over $\partial\Omega$ as f, i.e., $f = u|_{\partial\Omega}$. The inverse problem of our interest is then formulated as follows: given a single pair (g, f) of the Cauchy data or a small number (say 2 or 3) of pairs (g, f) for the system (1.1)-(1.2), we shall estimate the number and the supports D of the inhomogeneous media contained in the sampling domain Ω. We remark that, in general, the EIT problem refers to recovering the conductivity σ from the knowledge of the full Neumann-to-Dirichlet map Λ_σ, or in practice, from a good matrix approximation of such a map by measuring a large number of pairs (g, f) of the Cauchy data, say 32 or 64 pairs. However, in this work, we are mainly interested in the case when only one pair or two pairs (g, f) of Cauchy data is available. Theoretical aspects of medium reconstruction with one or few incidence currents are considered for example in [1, 2, 16], which affirmatively suggest this possibility. However, in practice, due to the limited data, we usually can not expect an accurate reconstruction of the conductivity profile, instead we intend to provide dome reasonable estimate of the number and the supports of all the inhomogeneities. We shall assume that the potential u is measured on the whole surface $\partial\Omega$ or on a part of $\partial\Omega$.

In this work, we propose a new direct sampling method (DSM) for solving the aforementioned EIT problem, which may fall into the vast category of the various direct methods developed in recent years [1, 2, 7, 8, 13, 20, 26, 30, 42]. We introduce a family of probing functions based on the dipole potential [4, 25]. We can then use these probing functions to define an indicator I, which provides the estimation of the supports of inhomogeneities inside Ω. This DSM is fast and computationally inexpensive, and it may serve as an ideal initialization for any more advanced and more expensive iterative optimization algorithms, e.g., [5, 9, 18, 19, 21, 35, 41, 46, 51, 56, 58], for further refinements of the numerical reconstruction. The

proposed DSM has a notable edge that it performs reasonably nice with a very limited set of measurement data, as confirmed by our numerical experiments. The principle of our DSM here for the EIT is similar to our earlier work in [32] which aims to solve the inverse acoustic medium scattering problem. However, the framework and techniques in this work are completely new.

The following is the outline of this work. In Section 2, we first introduce the general philosophy of a new DSM, then we propose a family of probing functions and an indicator for the new DSM to solve the EIT problem, as well as provide an alternative characterization of the indicator function, which helps us find an appropriate probing direction and analyze our probing method. We then verify some fundamental properties of the probing functions for our EIT problem in Section 3. In Section 4 we turn our attention to the domains Ω of special spherical geometry in $\mathbb{R}^n$ $(n = 2, 3)$ and use the Poincare-Steklov eigenvalue problem to explicitly derive the probing function for the cases, and discuss the properties of the probing function and the proposed indicator index. We then justify in Section 5 the optimality of the choice of the current densities to be used in our numerical experiments. In Section 6 we present some numerical experiments to demonstrate the effectiveness of our proposed DSM for the EIT problem with just one single pair or two pairs of Cauchy data.

2 Probing function and direct sampling method

2.1 General philosophy of direct sampling methods

In this section we shall first discuss the general philosophy of direct sampling methods. A direct sampling method was introduced and studied in [44] [49] using far-field data and in [32] using near-field data for locating inhomogeneities in inverse acoustic medium scattering. The method provides the location of the inhomogeneities based on an indicator function, which is defined as the L^2 inner product over the measurement surface between the measured data and the fundamental solution of the Helmholtz equation. Numerical experiments have shown that this method is effective and very robust to noise. It is particularly successful in locating multiple clustered objects sitting inside an acoustic medium with only a single or a few incident plane waves. The success of the method comes from the following two observations: the scattered field can be approximated by a finite sum of the fundamental solution of the Helmholtz equation centered at inhomogeneous inclusions; and the fundamental solutions centered at different points are nearly orthogonal in the L^2 inner product over the measurement surface.

These observations motivate our current development of DSMs to the EIT problem, when only one pair of Cauchy data is available. We shall construct an appropriate family of probing functions such that the scattered data can be approximated as a linear combination of these functions. Let (f, g) be a pair of Cauchy data measured over the surface $\partial\Omega$, i.e., $f = \Lambda_\sigma g$, with the Neumann-to-Dirichlet map Λ_σ defined as in (1.3). In the subsequent discussion, we shall often write $\Delta_{\partial\Omega}$ as the surface Laplace operator on $\partial\Omega$. Now we define the following duality product $\langle \cdot\,, \cdot \rangle_{\gamma,\partial\Omega}$:

$$\langle \chi, \phi \rangle_{\gamma,\partial\Omega} := \int_\Gamma (-\Delta_{\partial\Omega})^\gamma \chi\, \phi\, ds = \langle (-\Delta_{\partial\Omega})^\gamma \chi, \phi \rangle_{L^2(\partial\Omega)} \quad \text{for all } \chi \in H^{2\gamma}(\partial\Omega)\,, \phi \in L^2(\partial\Omega)\,, \tag{2.1}$$

with $\gamma \geq 0$. Clearly the space $L^2(\partial\Omega)$ can be considered as a subspace of the dual space of $H^{2\gamma}(\partial\Omega)$ in the following sense:

$$\langle \cdot\,, \phi \rangle_{\gamma,\partial\Omega} \in \left(H^{2\gamma}(\partial\Omega)\right)^* \quad \forall \phi \in L^2(\partial\Omega)\,. \tag{2.2}$$

For simplicity, we shall sometimes also write the duality product as $\langle \cdot\,, \cdot \rangle_\gamma$ when the domain of integration is clear in the context. The definition of the above duality product $\langle \cdot\,, \cdot \rangle_{\gamma,\partial\Omega}$ is advantageous in a sense that it is well-defined even when the function ϕ is merely an L^2 function. Let $|\cdot|_Y$ be a semi-norm respectively in the Sobelov space $H^{2\gamma}(\partial\Omega)$. Assume that we can select a family of probing functions $\{\eta_{x,d}\}_{x\in\Omega, d\in\mathbb{R}^n} \subset H^{2\gamma}(\partial\Omega)$ which satisfies the following two conditions:

(a) the family is nearly orthogonal with respect to $\langle \cdot, \cdot \rangle_{\gamma,\partial\Omega}$ and $|\cdot|_Y$, namely for any $y \in \Omega$ and $d_x, d_y \in \mathbb{R}^n$, the function

$$x \mapsto K_{d_x,d_y}(x,y) := \frac{\langle \eta_{x,d_x}, \eta_{y,d_y} \rangle_{\gamma,\partial\Omega}}{|\eta_{x,d_x}|_Y} \tag{2.3}$$

attains maximum at $x = y$ with a sharply peaked Gaussian like distribution. Here and throughout this work, a function that attains maximum at $x = y$ with a sharply peaked Gaussian like distribution refers to a function that behaves like a sharply peaked Gaussian kernel $\exp\left(-\frac{|x-y|^2}{4\sigma}\right)$ with small σ, namely it achieves the largest values when x is near the center y and decays rapidly when x moves away from y;

(b) the family of functions is fundamental, namely the scattered potential $f - \Lambda_{\sigma_0} g$ can be approximated by a linear combination of the probing functions in the following form:

$$(f - \Lambda_{\sigma_0} g)(\xi) = (\Lambda_\sigma g - \Lambda_{\sigma_0} g)(\xi) \approx \sum_k a_k \eta_{x_k,d_k}(\xi) \quad \forall\, \xi \in \partial\Omega\,, \tag{2.4}$$

where $\{x_k\}$ are some quadrature points sitting inside D, $d_k \in \mathbb{R}^n$ and a_k are some given vectors and coefficients respectively.

Under these assumptions, we are now ready to define the following index function

$$I(x, d_x) := C_1 \frac{\langle \eta_{x,d_x}, f - \Lambda_{\sigma_0} g \rangle_{\gamma,\partial\Omega}}{|\eta_{x,d_x}|_Y}\,, \quad x \in \Omega\,, d_x \in \mathbb{R}^n\,, \tag{2.5}$$

where C_1 is a constant independent of x and d_x. Then we derive from (2.4) and (2.5) that

$$I(x, d_x) \approx \sum_k C_1 a_k \frac{\langle \eta_{x,d_x}, \eta_{x_k,d_k} \rangle_{\gamma,\partial\Omega}}{|\eta_{x,d_x}|_Y} = \sum_k C_1 a_k K_{d_x,d_k}(x, x_k)\,, \tag{2.6}$$

where K_{d_x,d_k} is the function defined as in (2.3). From the above representation of the index function I, we can readily observe that the magnitude of the index is relatively large when x sits inside D, whereas it is relatively small otherwise. Hence, if we see that the magnitude of the index function I is relatively large at a point $x \in \Omega$, it is very likely that the point lies in D. Therefore the index function shall provide us with a good estimate of the number and supports of the inhomogeneous inclusions D inside Ω.

2.2 Probing functions for DSM

In this subsection, we shall introduce a family of probing functions $\{\eta_{x,d}\}_{x\in\Omega, d\in\mathbb{R}^n} \subset H^{2\gamma}(\partial\Omega)$ which we will use in the DSM for the EIT problem. For this purpose, we first define for any given $x \in \Omega$ and $d \in \mathbb{R}^n$ a function $w_{x,d}$ as the solution of the following equation

$$-\Delta w_{x,d} = -d \cdot \nabla \delta_x \quad \text{in} \quad \Omega\,; \quad \frac{\partial w_{x,d}}{\partial \nu} = 0 \quad \text{on} \quad \partial\Omega\,; \quad \int_{\partial\Omega} w_{x,d}\, ds = 0\,. \tag{2.7}$$

We readily see that the function $w_{x,d}$ is linear with respect to d. For any $x \in \Omega$ and $d \in \mathbb{R}^n$, it is easy to verify that the following dipole potential in the n-th dimension [4, 25]:

$$D_{x,d}(\xi) := c_n \frac{(x - \xi) \cdot d}{|x - \xi|^n}\,, \quad \xi \in \mathbb{R}^n \backslash \{x\}\,, \tag{2.8}$$

where c_n is a dimensionality constant, satisfies the equation in the entire space

$$-\Delta D_{x,d} = -d \cdot \nabla \delta_x \quad \text{in} \quad \mathbb{R}^n\,. \tag{2.9}$$

By subtracting the first equation in (2.7) from (2.9), we see that the difference $\varphi_{x,d} = D_{x,d} - w_{x,d}$ solves the following system

$$-\Delta\varphi_{x,d} = 0 \quad \text{in } \Omega\,; \quad \frac{\partial\varphi_{x,d}}{\partial\nu} = \frac{\partial D_{x,d}}{\partial\nu} \quad \text{on } \partial\Omega\,; \quad \int_{\partial\Omega}\varphi_{x,d}\,ds = \int_{\partial\Omega} D_{x,d}\,ds\,. \tag{2.10}$$

With the above notions, we are now ready to define a family of probing functions $\{\eta_{x,d}(\xi)\}_{x\in\Omega,d\in\mathbb{R}^n} \subset H^{2\gamma}(\partial\Omega)$ as the surface potential over $\partial\Omega$ created by w_x, i.e.,

$$\eta_{x,d}(\xi) := w_{x,d}(\xi)\,, \quad \xi \in \partial\Omega\,. \tag{2.11}$$

With the definition of the Neumann-to-Dirichlet map Λ_σ in (1.3), we can also write the function $\eta_{x,d}$ in the representation below

$$\eta_{x,d}(\xi) = D_{x,d}(\xi) - \left[\Lambda_1\left(\frac{\partial D_{x,d}}{\partial\nu}\right)\right](\xi) - C, \quad \xi \in \partial\Omega \tag{2.12}$$

where C is a constant such that

$$\int_{\partial\Omega}\eta_{x,d}\,ds = 0\,. \tag{2.13}$$

We will verify in sections 3 and 4 that this family of probing functions satisfy the two assumptions (2.3) and (2.4) stated in the previous subsection for some special and frequently used measurement surface $\partial\Omega$.

Actually, the application of the above family of dipole functions for solving the EIT problem is not new. Theoretical aspect of investigating the possibility of medium reconstruction by dipole functions is first considered in an notable work of [16]. An asymptotic formula for the steady-state voltage potential for a conductor with a finite number of well-separated and small inhomogeneities is derived in terms of polarization tensors (GT) and the derivative of Neumann function (hence the dipole). A L^∞-Lipschitz estimate of continuous dependence was also established, which provides a theoretical basis for identifiability and its performance with few incidence currents. Using the asymptotic relation and the estimate of continuous dependence, a reconstruction method was proposed for the EIT problem based on a minimization procedure. Full asymptotic expansions using the dipole and generalized polarization tensors (GPT) were then developed in [1, 2] with some theoretical investigation for the medium reconstruction from remote measurement. Based on these expansions several reconstruction methods are developed, for example, the GPTs matching approach under the level-set framework. The dipole probing function $\eta_{x,d}$ was also adopted in [42] to define an indicator function of the factorization method:

$$F(x) = \sum_{k=1}^{\infty} \frac{\langle \eta_{x,d}, v_k\rangle^2_{L^2(\partial\Omega)}}{\lambda_k}, \tag{2.14}$$

where (λ_k, v_k) are the eigen-pairs of the map Λ_σ defined as in (1.3). Assume that the conductivity coefficient σ is a piecewise constant function which attains the values σ_i, $i = 0, \ldots, N$, where σ_0 is the homogeneous background medium. Provided that all conductivities inside the inclusions satisfy either $\sigma_i > \sigma_0$ for all $i \neq 0$, or $\sigma_i < \sigma_0$ for all $i \neq 0$, then the series in (2.14) converges if and only if $x \in \Omega$ is outside the inclusions D. If there are only L pairs of Cauchy data available, we can only obtain an approximation of Λ_σ as an $L \times L$ matrix, and consequently only an approximation $F_L(x)$ of the series (2.14) as a sum of L terms. In practice, we need a practical criterion to determine if the series $F(x)$ converges. It is suggested in [11, 12, 13] to use a linear regression over the numerator and denominator of the terms in (2.14) and declare that the series converges if the numerator decays more rapidly than the denominator. As we may have noticed, in order to evaluate the above indicator function, many incident fields may be required and then a factorization of the $L \times L$ matrix is performed which approximates the operator Λ_σ.

On the other hand, we shall use this dipole function for a very different purpose in our DSM. We introduce the dipole potential as a family of probing functions, and use them to define an index function in the next subsection, which helps us estimate the supports of the inhomogeneous media D. The evaluation of our index function does not involve matrix factorizations or iterations, and it can be carried out with a single or a very small number of incident fields.

2.3 Index function for DSM

In this subsection, we shall introduce an index function for solving the EIT problem based on the family of dipole functions $\{\eta_{x,d}\}_{x\in\Omega, d\in\mathbb{R}^n}$ introduced in the last section.

For the ease of exposition, we shall focus on the duality product $\langle\cdot\,,\cdot\rangle_{2,\partial\Omega}$, and consider $|\cdot|_Y$ to be the semi-norm of $H^{3/2}(\partial\Omega)$. If we choose C_1 to be a normalization constant $1/||f-\Lambda_{\sigma_0}g||_{L^2(\partial\Omega)}$, and substitute these expressions into (2.5), we come up with the following expression of the index function for $x\in\Omega$ and $d_x\in\mathbb{R}^n$:

$$I(x,d_x) := \frac{\langle \eta_{x,d_x}, f-\Lambda_{\sigma_0}g\rangle_{2,\partial\Omega}}{||f-\Lambda_{\sigma_0}g||_{L^2(\partial\Omega)}|\eta_{x,d_x}|_{H^{\frac{3}{2}}(\partial\Omega)}}\,, \quad x\in\Omega\,, d_x\in\mathbb{R}^n\,. \tag{2.15}$$

One point to note is that, with our definition of the duality product $\langle\cdot\,,\cdot\rangle_{2,\mathbb{S}^1}$ in (2.1), the surface Laplace operator is only acting on the probing function $\eta_{x,d}$ (on the left-hand side of the duality product) which is itself infinitely smooth over the measurement surface, and therefore (2.15) makes sense even when $f-\Lambda_{\sigma_0}g$ contains noise and is merely in L^2. The noise enters the index function directly and is smoothed by the duality product via integration over the measurement surface. This may provide a reason for the robustness of our DSM against noise that we have observed from our numerical experiments in Section 6 when the index function (2.15) is used to locate inhomogeneities in a sampling domain.

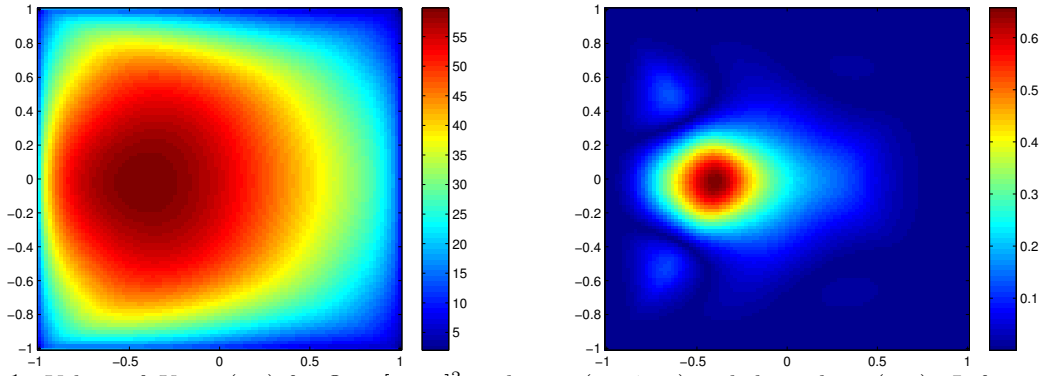

Figure 1: Values of $K_{d_x,d_y}(\cdot,y)$ for $\Omega=[-1,1]^2$ with $y=(-0.41,0)$ and $d_x=d_y=(0,1)$. Left: $\gamma=0$ and $|\cdot|_Y=|\cdot|_{L^2}$; right: $\gamma=2$ and $|\cdot|_Y=|\cdot|_{H^{3/2}}$.

Actually, the introduction of the duality product $\langle\cdot\,,\cdot\rangle_{\gamma,\partial\Omega}$ in the above index function is motivated from the following intuitive observation. From the fact that $\Delta w_x=0$ near the boundary $\partial\Omega$, we have

$$-\Delta_{\partial\Omega}\eta_x = \frac{\partial^2 w_x}{\partial\nu^2} + g(\partial)w_x\,, \tag{2.16}$$

where $g(\partial)$ is a first order differential operator. Therefore for any $\gamma\geq 0$, we have

$$(-\Delta_{\partial\Omega})^{\gamma}\eta_x = \left(\frac{\partial}{\partial\nu}\right)^{2\gamma} w_x + h(\partial)w_x\,, \tag{2.17}$$

where $h(\partial)$ is a pseudo-differential operator of order less than 2γ. Therefore, we can observe that the action of $(-\Delta_{\partial\Omega})^{1/2}$ on the functions along the boundary is equivalent to taking the normal derivative at

the boundary up to a lower order term. Hence, the introduction of the duality product $\langle \cdot, \cdot \rangle_{\gamma,\partial\Omega}$ gives more sensitivity of the index function for the data. From our numerical experiments, we can actually observe that the kernel $K_{d_x,d_y}(\cdot, y)$ provides a much sharper distribution with $\gamma = 2$ and $|\cdot|_Y$ being the $H^{3/2}(\partial\Omega)$ semi-norm than $\gamma = 0$ and $|\cdot|_Y$ being the L^2-norm (see Figure 1), therefore significantly improves the performance of the index function to locate the inhomogeneities. These observations will be further confirmed in section 2.4 and 4 for some special domains Ω.

2.4 An alternative characterization of index function

In this subsection, we shall give an alternative characterization of the index function $I(x, d_x)$ defined in (2.15). With this representation of the index function, we can find an optimal probing direction $d_x \in \mathbb{R}^n$ for the index function at each point of $x \in \Omega$. We now define an auxiliary function which will be very useful to our subsequent discussion. Suppose that $f - \Lambda_{\sigma_0} g \in H^\alpha(\partial\Omega)$ for some $\alpha \geq \frac{1}{2}$. For a $\gamma \geq 0$ such that $2\alpha - 4\gamma \geq -1$, let ϕ be the solution to the following system:

$$-\Delta\phi = 0 \quad \text{in } \Omega\,; \quad \frac{\partial\phi}{\partial\nu} = (-\Delta_{\partial\Omega})^\gamma (f - \Lambda_{\sigma_0} g) \quad \text{on } \partial\Omega\,; \quad \int_{\partial\Omega} \phi\, ds = 0\,. \tag{2.18}$$

Then, from the Green's identity, we have that

$$\int_\Omega (w_{x,d_x}\Delta\phi - \phi\Delta w_{x,d_x})\, dx = \int_{\partial\Omega} \left(\eta_{x,d_x} \frac{\partial\phi}{\partial\nu} - \phi \frac{\partial w_{x,d_x}}{\partial\nu} \right) ds\,, \tag{2.19}$$

where w_{x,d_x} is defined as in (2.7) for $x \in \Omega, d_x \in \mathbb{R}^n$. From the definition of w_{x,d_x} in (2.7) and ϕ in (2.18), we therefore derive the following equation:

$$d_x \cdot \nabla\phi(x) = \int_{\partial\Omega} \eta_{x,d_x} \frac{\partial\phi}{\partial\nu}\, ds = \int_{\partial\Omega} \eta_{x,d_x} (-\Delta_{\partial\Omega})^\gamma (f - \Lambda_{\sigma_0} g)\, ds\,. \tag{2.20}$$

Noting that $f - \Lambda_{\sigma_0} g \in H^\alpha(\partial\Omega) \subset H^\gamma(\partial\Omega)$ and $\partial\Omega$ is a smooth closed surface, we arrive at, by comparing the above equation with (2.1), the following for all $x \in \Omega, d_x \in \mathbb{R}^n$,

$$\langle \eta_{x,d_x}, f - \Lambda_{\sigma_0} g \rangle_{\gamma,\partial\Omega} = \int_{\partial\Omega} (-\Delta_{\partial\Omega})^\gamma \eta_{x,d_x} (f - \Lambda_{\sigma_0} g)\, ds = d_x \cdot \nabla\phi(x)\,. \tag{2.21}$$

Then we can see, by comparing the definition (2.15) of the index function with the above relation, that

$$I(x, d_x) = \frac{d_x \cdot \nabla\phi(x)}{||f - \Lambda_{\sigma_0} g||_{L^2(\partial\Omega)} |\eta_{x,d_x}|_{H^{\frac{3}{2}}(\partial\Omega)}}\,, \quad x \in \Omega\,, d_x \in \mathbb{R}^n\,, \tag{2.22}$$

where ϕ is defined as in (2.18) with $\gamma = 2$. So we know the index function is maximized when d_x is chosen to be $d_x = \frac{\nabla\phi(x)}{|\nabla\phi(x)|}$ for each $x \in \Omega$. From the definition of the probing function η_{x,d_x} in (2.7), we can easily see that $\eta_{x,d_x} = \sum_{i=1}^n d_i \eta_{x,e_i}$, where $d_x = (d_1, d_2, \cdots, d_n)$ and e_i is an orthonormal basis in $\mathbb{R}^n$. Therefore the probing direction d_x can be selected pointwise cost-effectively for numerical purpose. As we observe from numerical experiments, such a choice of d_x may effectively avoid accidental removal of existing inhomogeneities in the reconstructed image when one might wrongly choose a probing direction which is orthogonal to $\nabla\phi(x)$ at a point $x \in \Omega$.

3 Verification of the fundamental property

In this section we shall show that the scattered potential in the EIT problem, $f - f_0 := \Lambda_\sigma g - \Lambda_{\sigma_0} g$, can be written as a finite sum as in (2.4) of the functions $w_{x,d}$ defined in (2.7). In the subsequent discussion, we shall often write u_0 to be the incident potential satisfies the following homogeneous equation

$$-\Delta u_0 = 0 \quad \text{in} \quad \Omega\,; \quad \sigma_0 \frac{\partial u_0}{\partial\nu} = g \quad \text{on} \quad \partial\Omega\,; \quad \int_{\partial\Omega} u_0\, ds = 0\,. \tag{3.1}$$

Comparing the above system with (1.1)-(1.2), we can see from (1.3) that $f_0 = \Lambda_{\sigma_0} g = u_0|_{\partial\Omega}$. We shall also let G_x to be the Green's function of $-\Delta$ with Neumann boundary condition, namely

$$-\Delta G_x = \delta_x \quad \text{in} \quad \Omega\,; \quad \frac{\partial G_x}{\partial \nu} = \frac{1}{|\partial\Omega|} \quad \text{on} \quad \partial\Omega\,; \quad \int_{\partial\Omega} G_x\, ds = 0\,. \tag{3.2}$$

From (2.11), we can see that our probing function $\eta_{x,d} = w_{x,d}$ on the boundary $\partial\Omega$. Therefore, comparing (3.2) with (2.7), we can readily verify that

$$\eta_{x,d}(\xi) = -d \cdot \nabla G_x(\xi)\,, \quad \xi \in \partial\Omega\,. \tag{3.3}$$

This follows directly from the fact that

$$-\Delta(-d \cdot \nabla G_x(\xi)) = d \cdot \nabla(\Delta G_x(\xi)) = -d \cdot \nabla \delta_x. \tag{3.4}$$

In the next two subsections, we will demonstrate the fundamental property (2.4) for the following two important cases: σ is a piecewise constant function, and σ is a smooth function.

3.1 Medium with piecewise constant inhomogeneities

Suppose that the coefficient σ in (1.1) is a piecewise constant function and that the support D of the function $\sigma - \sigma_0$ is in the form of $D = \overline{\bigcup_{i=1}^m \Omega_i} \Subset \Omega$ where Ω_i is an open domain representing the i-th open inclusion sitting inside Ω for $i = 1, \cdots, m$. For notational sake, we shall often write $\Omega_0 := \Omega \backslash D$. Assume that σ takes the value σ_i inside each of the domain Ω_i. Then we can readily derive from the potential equation (1.1) of u that for any $\phi \in H^1(\Omega)$,

$$0 = \sum_{i=0}^m \int_{\Omega_i} \sigma_i \nabla u \cdot \nabla \phi\, dx + \int_{\partial\Omega} g\phi\, ds = -\sum_{i=0}^n \int_{\Omega_i} \sigma_i \phi \Delta u\, dx + \sum_{i=1}^m \int_{\partial\Omega_i} \left(\sigma_i \frac{\partial u^-}{\partial \nu} - \sigma_0 \frac{\partial u^+}{\partial \nu} \right) \phi\, ds.$$

Here and through this paper, the superscripts $\pm$ indicates the limits from outside and inside of the domains Ω_i for $i = 1, \cdots, m$. Let the function $v := \sigma u$, then we get from the above and (1.2) that v satisfies the following system

$$-\Delta v = 0 \quad \text{in} \quad \Omega \backslash \left(\bigcup_{i=1}^m \partial\Omega_i \right)\,; \quad \frac{\partial v}{\partial \nu} = g \quad \text{in} \quad \partial\Omega\,; \quad \left.\frac{\partial v^-}{\partial \nu}\right|_{\partial\Omega_i} = \left.\frac{\partial v^+}{\partial \nu}\right|_{\partial\Omega_i}\,; \quad \int_{\partial\Omega} v\, ds = 0\,. \tag{3.5}$$

Moreover, we notice that the flux of v is continuous, i.e. $[\frac{\partial v}{\partial \nu}] = \frac{\partial v^+}{\partial \nu} - \frac{\partial v^-}{\partial \nu} = 0$, whereas the function v is itself discontinuous, i.e. its jump $[v] := v^+ - v^-$ is non-zero. Define the function $\eta := \sigma u - \sigma_0 u_0$ where u_0 satisfies (3.1), then we can see from the above and (3.1) that η satisfies the following system

$$-\Delta \eta = 0 \quad \text{in} \quad \Omega \backslash \left(\bigcup_{i=1}^m \partial\Omega_i \right)\,; \quad \frac{\partial \eta}{\partial \nu} = 0 \quad \text{in} \quad \partial\Omega\,; \quad \int_{\partial\Omega} \eta\, ds = 0\,, \tag{3.6}$$

with further properties that $[\eta] = [v]$ and $[\frac{\partial \eta}{\partial \nu}] = [\frac{\partial v}{\partial \nu}] = 0$ on $\partial\Omega_i$. Therefore, combining the above several properties of the function η, we can deduce the following expression from the Green's representation and (3.2), (3.6) that, for any $\xi \in \Omega_0$,

$$\begin{aligned}
\eta(\xi) &= \int_{\partial\Omega} \left(G_\xi \frac{\partial \eta}{\partial \nu} - \eta \frac{\partial G_\xi}{\partial \nu} \right) ds + \sum_{i=1}^m \int_{\partial\Omega_i} \left(G_\xi \frac{\partial \eta^+}{\partial \nu} - \eta^+ \frac{\partial G_\xi}{\partial \nu} \right) ds \\
&= \int_{\partial\Omega} \left(G_\xi \frac{\partial \eta}{\partial \nu} - \eta \frac{\partial G_\xi}{\partial \nu} \right) ds + \sum_{i=1}^m \int_{\partial\Omega_i} \left(G_\xi \frac{\partial \eta^-}{\partial \nu} - \eta^- \frac{\partial G_\xi}{\partial \nu} \right) ds - \sum_{i=1}^m \int_{\partial\Omega_i} [\eta] \frac{\partial G_\xi}{\partial \nu}\, ds \\
&= -\sum_{i=1}^m \int_{\partial\Omega_i} [\eta] \frac{\partial G_\xi}{\partial \nu}\, ds\,.
\end{aligned} \tag{3.7}$$

Since η is continues near $\partial\Omega$, and that $\eta = u - u_0$ on $\partial\Omega$, we have the following representation of the scattered field for $\xi \in \partial\Omega$,

$$(f - f_0)(\xi) = (u - u_0)(\xi) = \eta(\xi) = -\sum_{i=1}^{m} \int_{\partial\Omega_i} [\eta] \frac{\partial G_\xi}{\partial \nu}\, ds\,. \tag{3.8}$$

From the above representation and numerical quadrature rule, we can therefore approximate the scattered potential $f - f_0$ by a finite sum of probing functions as follows

$$(f - f_0)(\xi) \approx \sum_k a_k \eta_{x_k, d_k}(\xi)\,, \quad \xi \in \partial\Omega\,, \tag{3.9}$$

where x_k are some quadrature points located along $\bigcup_{i=1}^m \partial\Omega_i \subset D$, a_k are some coefficients, and $d_k = \nu(x_k) \in \mathbb{R}^n$. Therefore property (2.4) follows when σ is a piecewise constant function.

3.2 Medium with smooth conductivity

In this subsection, we assume the coefficient σ in (1.1) to be a $C^{1,\alpha}$ function with $0 < \alpha < 1$ and $D \Subset \Omega$. Then we know the solution u of the potential equation (1.1) is in $C^{2,\alpha}$. Subtracting (3.1) from (1.1),

$$\sigma_0 \Delta(u - u_0) + \nabla \cdot ((\sigma - \sigma_0)\nabla u) = 0 \quad \text{in} \quad \Omega\,; \quad \frac{\partial (u - u_0)}{\partial \nu} = 0 \quad \text{on} \quad \partial\Omega\,; \quad \int_{\partial\Omega} (u - u_0)\, ds = 0\,. \tag{3.10}$$

We further deduce from the Green's representation theorem and (3.2), (3.10) the following for all $\xi \in \Omega$,

$$\begin{aligned} 0 &= -\int_\Omega (\sigma - \sigma_0)\nabla u \cdot \nabla G_\xi\, dx + \sigma_0 \int_\Omega G_\xi \Delta(u - u_0)\, dx \\ &= -\int_\Omega (\sigma - \sigma_0)\nabla u \cdot \nabla G_\xi\, dx - \sigma_0 (u - u_0)(\xi) - \sigma_0 \int_{\partial\Omega} (u - u_0) \frac{\partial G_\xi}{\partial \nu}\, ds \\ &= -\int_\Omega (\sigma - \sigma_0)\nabla u \cdot \nabla G_\xi\, dx - \sigma_0 (u - u_0)(\xi)\,. \end{aligned} \tag{3.11}$$

Since $u - u_0$ is continues near the boundary $\partial\Omega$, we get from the above equality that for all $\xi \in \partial\Omega$,

$$(f - f_0)(\xi) = (u - u_0)(\xi) = -\frac{1}{\sigma_0} \int_D (\sigma - \sigma_0)\nabla u \cdot \nabla G_\xi\, dx\,. \tag{3.12}$$

Therefore, from the above representation and numerical quadrature rule, we can approximate the scattered potential $f - f_0$ by a finite sum of probing functions as follows

$$(f - f_0)(\xi)(\xi) \approx \sum_k a_k \eta_{x_k, d_k}(\xi)\,, \quad \xi \in \partial\Omega\,, \tag{3.13}$$

where x_k are some quadrature points located in D, a_k are some coefficients, and $d_k = \nabla u(x_k) \in \mathbb{R}^n$. This validates the fundamental property (2.4) for the case when σ is a smooth function.

4 Explicit formulae for probing functions and index function

In the previous sections, we have discussed our probing method and techniques that we use in the DSM for the EIT problem for a general domain Ω. From now on, we turn our attention to another interesting topic, namely, we come to some special cases of the domain Ω to work out the analytical expressions for both the probing functions and their duality products $\langle \cdot, \cdot \rangle_{\gamma, \partial\Omega}$, therefore the distribution kernel K defined in (2.3). We consider the two cases: $\Omega = B_1(0) := \{x \in \mathbb{R}^n;\ |x| < 1\} \subset \mathbb{R}^n$ for $n = 2, 3$. Such spherical geometric shapes are popular ones for measurement surfaces in applications. These analytical

expressions of the probing functions and duality products help us to understand the behaviour of the distribution kernel K and thus the index function I in (2.15). We may also observe from these analytical expressions that, in these special cases, the family of probing functions is nearly orthogonal with respect to $\langle \cdot, \cdot \rangle_{\gamma,\partial\Omega}$ and $|\cdot|_Y$ as stated in section 2, namely for any $y \in \Omega$ and $d_x, d_y \in \mathbb{R}^n$, the function

$$x \mapsto K_{d_x,d_y}(x,y) := \frac{\langle \eta_{x,d_x}, \eta_{y,d_y} \rangle_{\gamma,\partial\Omega}}{|\eta_{x,d_x}|_Y} \tag{4.1}$$

attains maximum at $x = y$ with a sharply peaked Gaussian like distribution. For this purpose, we first calculate the eigenvalues and eigenfunctions of the Neumann-to-Dirichlet map Λ_σ for thse special domains Ω. In fact, explicit calculations of these eigenvalue and eigenfunctions and related research have been investigated in [11, 14, 48]. However, since these results are of fundamental importance in obtaining formulae for the probing functions and their duality products, we would like to briefly go through some of these results below.

4.1 Poincare-Steklov eigenvalue problem

Let Λ_σ be defined as in (1.3). We know that Λ_σ is a compact self-adjoint operator in $L^2(\partial\Omega)$, so by the Hilbert-Schmidt theorem, there exists a complete orthogonal basis $\{v_m\}_{m\in\mathbb{N}}$ such that $\Lambda_\sigma v_m = \lambda_m v_m$ with $\lambda_m \to 0$ if $m \to \infty$. In this section we shall find the explicit formulae for the eigenpairs (λ_m, v_m) when the domain is a unit disk $\Omega = B_1(0) \subset \mathbb{R}^2$ and the conductivity distribution is piecewise constant in the radial direction. For this purpose, let us first consider the following conductivity distribution:

$$\sigma(x) = \begin{cases} \kappa & \text{for } |x| \le \rho\,, \\ \\ 1 & \text{for } \rho < |x| < 1\,, \end{cases} \tag{4.2}$$

with κ and ρ being two positive constants. Now we consider the current g in (1.1) to be of the form $g(x) = e^{im\theta}$ where $x = (1,\theta) \in \mathbb{S}^1 = \partial B_1(0)$ and $m \in \mathbb{Z}\backslash\{0\}$. Then, following the same arguments as in [48], rewriting equation (1.1) in polar coordinates, we can derive the following expansions of the eigenpairs of Λ_σ:

$$\lambda_m = \frac{1}{m}\frac{1-\rho^{2m}\mu}{1+\rho^{2m}\mu}, \quad v_m = \frac{1}{\sqrt{2\pi}}\cos m\theta \quad \text{or} \quad \frac{1}{\sqrt{2\pi}}\sin m\theta \quad \text{for } m \in \mathbb{N}\backslash\{0\}\,. \tag{4.3}$$

where $\mu = (1-\sqrt{\kappa})/(1+\sqrt{\kappa})$. In particular, if $\sigma \equiv 1$ in Ω, we have the simplified eigenpairs in (4.3) with $\mu = 0$, and the corresponding solution to the system (1.1) when $g(x) = e^{im\theta}$ for $m \in \mathbb{Z}\backslash\{0\}$ is given by

$$u_m(x) = \frac{r^{|m|}}{|m|}e^{im\theta}\,, \quad x \in \Omega \tag{4.4}$$

A similar result can be derived for $\Omega = B_1(0) \subset \mathbb{R}^3$ with the help of the spherical harmonics.

Using the above eigenpairs of Λ_σ, we are now ready to explicitly construct some probing functions.

4.2 Probing functions for circular domains

In this subsection we shall explicitly calculate, for a given $x \in \Omega$ and $d \in \mathbb{R}^n$, the probing function $\eta_{x,d}$ defined in (2.11) for the unit circular domain, namely $\Omega = B_1(0)$ in $\mathbb{R}^2$ and when the homogeneous background coefficient $\sigma_0 = 1$. The results can be easily extended to the general circular domains or when the homogeneous background coefficient $\sigma_0 \neq 1$. For this purpose, we first consider, for any smooth function ψ on $\partial\Omega$, the solution φ to the following Neumann problem:

$$-\Delta\varphi = 0 \quad \text{in } \Omega\,; \quad \frac{\partial\varphi}{\partial\nu} = \psi \quad \text{on } \partial\Omega\,; \quad \int_{\partial\Omega}\varphi\, ds = 0. \tag{4.5}$$

Since φ is smooth, we have, from the Green's identity and the definition of $w_{x,d}$ in (2.7), that

$$-\int_{\partial\Omega}\frac{\partial\varphi}{\partial\nu}w_{x,d}\,ds=\int_{\partial\Omega}\left(\frac{\partial w_{x,d}}{\partial\nu}\varphi-\frac{\partial\varphi}{\partial\nu}w_{x,d}\right)ds=\int_{\Omega}\left(\varphi\Delta w_{x,d}-w_{x,d}\Delta\varphi\right)dy=-d\cdot\nabla\varphi(x). \tag{4.6}$$

Putting (2.11) and (4.5) into the above equality, we get that

$$\int_{\partial\Omega}\psi\eta_{x,d}\,ds=d\cdot\nabla\varphi(x)\,. \tag{4.7}$$

From section 4.1, we can see that, for $m\in\mathbb{Z}\backslash\{0\}$, if $\psi=e^{im\theta}$ with $\theta\in(0,2\pi]$ is the boundary condition in (4.5), then from the discussion of the Poincare-Steklov eigenlaue problem in the last subsection, the solution φ to the system (4.5) is actually given by $\varphi=u_m=\frac{r^{|m|}}{|m|}e^{im\theta}$. Therefore we get that

$$\int_{\mathbb{S}^1}\eta_{x,d}(\theta)e^{im\theta}\,ds=d\cdot\nabla\left(\frac{r_x^{|m|}}{|m|}e^{im\theta_x}\right), \tag{4.8}$$

where $x=(r_x,\theta_x)$ is in the polar coordinate. We recall the Fourier coefficients $\mathfrak{F}(g)$ of $g\in L^2(\mathbb{S}^1)$:

$$[\mathfrak{F}(g)](m)=\frac{1}{\sqrt{2\pi}}\int_0^{2\pi}g(\theta)e^{-im\theta}\,d\theta\,,\quad m\in\mathbb{Z}. \tag{4.9}$$

Comparing (4.8) with (4.9), and from the fact that the probing function $\eta_{x,d}$ has zero mean, we obtain

$$[\mathfrak{F}(\eta_{x,d})](m)=\frac{1}{\sqrt{2\pi}}d\cdot\nabla\left(\frac{r^{|m|}}{|m|}e^{-im\theta}\right)\quad\forall m\in\mathbb{Z}\backslash\{0\}\,;\quad[\mathfrak{F}(\eta_{x,d})](0)=0\,, \tag{4.10}$$

which directly gives, for $m\neq0$,

$$[\mathfrak{F}(\eta_{x,d})](m)=\begin{cases}e^{-i(\theta_d-\theta_x)}r_x^{|m|-1}e^{-im\theta_x} & \text{if } m>0,\\ e^{i(\theta_d-\theta_x)}r_x^{|m|-1}e^{-im\theta_x} & \text{if } m<0.\end{cases} \tag{4.11}$$

With some basic calculations, we can then deduce the following explicit expression for $\eta_{x,d}$:

$$\eta_{x,d}(\xi)=\frac{1}{\pi}\frac{(\xi-x)\cdot d}{|x-\xi|^2}\,,\qquad\text{for }\xi\in\mathbb{S}^1. \tag{4.12}$$

Similarly, we may also calculate explicitly the duality product $\langle\,\cdot\,,\,\cdot\,\rangle_\gamma$ between the probing functions which lie in $H^\gamma(\partial\Omega)$ with $\gamma\geq0$. Since the complete orthonomal set $\{e^{im\theta}\}_{m\in\mathbb{Z}}$ in $L^2(0,2\pi)$ are the eigenfunctions of the surface Laplacian operator $-\Delta_{\mathbb{S}^1}$ with each of their corresponding eigenvalues as m^2, the definition of the duality product $\langle\,\cdot\,,\,\cdot\,\rangle_{\gamma,\mathbb{S}^1}$ on $\mathbb{S}^1$ (see (2.1)) between η_{x,d_x} and η_{y,d_y} gives

$$\langle\eta_{x,d_x},\eta_{y,d_y}\rangle_{\gamma,\mathbb{S}^1}=\sum_{m\in\mathbb{Z}}m^{2\gamma}\overline{[\mathfrak{F}(\eta_{x,d_x})](m)}[\mathfrak{F}(\eta_{y,d_y})](m)\,. \tag{4.13}$$

Substituting (4.11) into the above expression, we have for any $\gamma\geq0$,

$$\langle\eta_{x,d_x},\eta_{y,d_y}\rangle_{\gamma,\mathbb{S}^1}=2\mathrm{Re}\left(e^{i(\theta_{d_x}-\theta_{d_y}-\theta_x+\theta_y)}\sum_{m=1}^{\infty}m^{2\gamma}(r_xr_y)^{m-1}e^{im(\theta_x-\theta_y)}\right), \tag{4.14}$$

where $x=(r_x,\theta_x)$, $y=(r_y,\theta_y)$, $d_x=(r_{d_x},\theta_{d_x})$ and $d_x=(r_{d_x},\theta_{d_x})$ are in their polar coordinates. This directly gives the $H^\gamma(\mathbb{S}^1)$ Sobolov semi-norms of η_{x,d_x}:

$$|\eta_{x,d_x}|^2_{\gamma,\mathbb{S}^1}=2\sum_{m=1}^{\infty}m^{2\gamma}r_x^{2m-2}\,, \tag{4.15}$$

We now calculate the above two series explicitly for $2\gamma \in \mathbb{N}$. For this purpose, we define an auxiliary function $G^\beta(z)$. For $z \in \mathbb{C}$ such that $|z| < 1$, $G^\beta(z)$ is defined for all $\beta \in \mathbb{N}$ by

$$G^\beta(z) \quad := \quad \left(z\frac{\partial}{\partial z}\right)^\beta \left(\frac{1}{1-z}\right) = \sum_{m=0}^{\infty} m^\beta z^m \,, \tag{4.16}$$

which holds true since the series converges absolutely, and can be explicitly calculated for any $\beta \in \mathbb{N}$ recursively using expression (4.16). Comparing the above function with (4.15), we have

$$|\eta_{x,d_x}|^2_{0,\mathbb{S}^1} = 2G^0(r_x^2)\,, \quad |\eta_{x,d_x}|^2_{\gamma,\mathbb{S}^1} \quad = \quad \frac{2}{r_x^2}G^\gamma(r_x^2) \quad \text{for } \gamma > 0\,, \tag{4.17}$$

which yields, for instance,

$$|\eta_{x,d_x}|^2_{0,\mathbb{S}^1} = \frac{2}{1-r_x^2}\,, \quad |\eta_{x,d_x}|^2_{\frac{1}{2},\mathbb{S}^1} = \frac{2}{(1-r_x^2)^2}\,, \quad |\eta_{x,d_x}|^2_{1,\mathbb{S}^1} = \frac{2(1+r_x^2)}{(1-r_x^2)^3}\,.$$

This gives an explicit formula for calculation of the $H^\gamma(\mathbb{S}^1)$ Sobolov semi-norms of η_{x,d_x} for $2\gamma \in \mathbb{N}$. Whereas, for the duality product $\langle\,\cdot\,,\,\cdot\,\rangle_{\gamma,\mathbb{S}^1}$, a direct comparison between the function (4.16) with (4.14) gives, for $\gamma = 0$, that

$$\langle \eta_{x,d_x}, \eta_{y,d_y}\rangle_{0,\mathbb{S}^1} = \frac{2\cos(\theta_{d_x}-\theta_{d_y}) - 2r_xr_y\cos(\theta_{d_x}-\theta_{d_y}-\theta_x+\theta_y)}{1-2r_xr_y\cos(\theta_x-\theta_y)+r_x^2r_y^2}, \tag{4.18}$$

while, for $\gamma > 0$, that

$$\langle \eta_{x,d_x}, \eta_{y,d_y}\rangle_{\gamma,\mathbb{S}^1} \quad = \quad 2\mathrm{Re}\left(\frac{e^{i(\theta_{d_x}-\theta_{d_y}-\theta_x+\theta_y)}}{r_xr_y}G^{2\gamma}(r_xr_ye^{i(\theta_x-\theta_y)})\right) \tag{4.19}$$

which yields, for instance, the duality product $\langle\,\cdot\,,\,\cdot\,\rangle_{\frac{1}{2}}$ as:

$$\langle \eta_{x,d_x}, \eta_{y,d_y}\rangle_{\frac{1}{2},\mathbb{S}^1} = \frac{2\cos(\theta_{d_x}-\theta_{d_y}) - 4r_xr_y\cos(\theta_{d_x}-\theta_{d_y}-\theta_x+\theta_y) + 2r_x^2r_y^2\cos(\theta_{d_x}-\theta_{d_y}-2\theta_x+2\theta_y)}{\left(1-2r_xr_y\cos(\theta_x-\theta_y)+r_x^2r_y^2\right)^2}.$$

This gives an explicit formula for computing the duality product $\langle\,\cdot\,,\,\cdot\,\rangle_\gamma$ of η_{x,d_x} for $2\gamma \in \mathbb{N}$. Although the four terms x, y, d_x, d_y in the duality products are deeply coupled, we can see by substituting (4.17) and (4.18)-(4.19) into (2.3) that the kernel (2.3) attains maximum when x is near y and when $d_x \approx d_y$, and that it gives a sharper peak as γ increases. This justifies the validity of the DSM for EIT for the circular domain. We show, as an example, the values of the duality products $\langle\,\cdot\,,\,\cdot\,\rangle_\gamma$ between the probing functions for $\gamma = 0$; see Figure 2 (Left); and $\gamma = \frac{1}{2}$; see Figure 2 (Right).

4.3 Probing function for an open ball

In this subsection we shall construct the probing function $\eta_{x,d}$ defined in (2.11) for $x \in \Omega$ and $d \in \mathbb{R}^n$ when Ω is an open ball $\Omega = B_1(0) \subset \mathbb{R}^3$ and $\sigma_0 = 1$. Same as in the previous section, the result can be easily extended to the general open balls or the case with $\sigma_0 \neq 1$. In order to construct the probing function, for any smooth function ψ over the boundary $\partial\Omega$, we first consider the function φ to be the solution to (4.5) when Ω is now replaced by the ball $B_1(0)$: with the same argument as in the previous section, we again apply the Green's identity to get equation (4.7) with this new domain. Next, we would like to choose a set of smooth functions ψ over $\mathbb{S}^2$ in (4.5) so as to obtain enough information to construct the probing function $\eta_{x,d}$. For this purpose, we consider the set of spherical harmonics on $\mathbb{S}^2$, for any $l \in \mathbb{Z}, -m \leq l \leq m$,

$$Y_l^m(\theta,\phi) := \sqrt{\frac{(2l+1)(l-m)!}{(l+m)!}}P_l^m(\cos(\theta))e^{im\phi}\,, \tag{4.20}$$

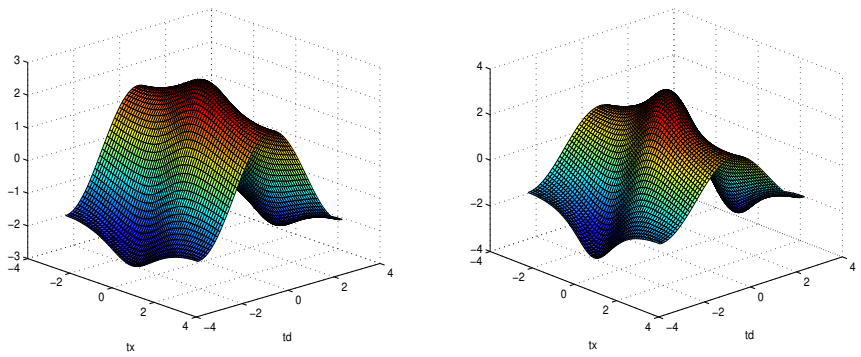

Figure 2: The values of duality products $\langle \cdot, \cdot \rangle_\gamma$ between the probing functions for $\gamma = 0$ (Left) and $\gamma = \frac{1}{2}$ (right) when $tx := \theta_x - \theta_y \in (-\pi, \pi)$ and $td := \theta_{d_x} - \theta_{d_y} \in (-\pi, \pi)$, $r_x = 0.5$, $r_y = 0.4$.

where $(\theta, \phi) \in (-\pi, \pi) \times (0, 2\pi)$ and P_l^m are the associated Legendre polynomials. From the fact that the family of $\{Y_l^m(\theta, \phi)\}_{l \in \mathbb{Z}, -m \le l \le m}$ form a complete orthonormal set in $L^2(\mathbb{S}^2)$ and that the function $\eta_{x,d}$ has a zero mean along $\mathbb{S}^2$, we have for $\xi \in \mathbb{S}^2$ that

$$\eta_{x,d}(\xi) = \frac{1}{\sqrt{4\pi}} \sum_{l=1}^{\infty} \sum_{m=-l}^{l} (g_{x,d})_{l,m} Y_l^m(\theta, \phi)\,, \tag{4.21}$$

where $x = (\theta, \phi)$ and the coefficients $(g_{x,d})_{l,m}$ are defined by

$$(g_{x,d})_{l,m} := \frac{1}{\sqrt{4\pi}} \int_{\mathbb{S}^2} \eta_{x,d}(\theta, \phi) \overline{Y_l^m(\theta, \phi)} ds\,. \tag{4.22}$$

If we let $\psi(\theta, \phi) = Y_l^m(\theta, \phi)$ in (4.5) with Ω replaced by $B_1(0)$ in $\mathbb{R}^3$, then by separation of variables, we derive the following formula for the solution φ to (4.5):

$$\varphi(\xi) = \frac{r^l}{l} Y_l^m(\theta, \phi) \quad \forall\, \xi \in B_1(0),$$

where $\xi = (r, \theta, \phi)$ is in its spherical coordinate. Therefore, we deduce by substituting the above expression and (4.7) into (4.22) that

$$(g_{x,d})_{l,m} = \frac{1}{\sqrt{4\pi}} \int_{\mathbb{S}^2} \eta_{x,d}(\theta, \phi) \overline{Y_l^m(\theta, \phi)} ds = d \cdot \nabla_k \left(\frac{r_k^l}{l} \overline{Y_l^m(\theta_k, \phi_k)} \right) \Big|_{k=x}. \tag{4.23}$$

Now from (4.7) and the above expression the coefficients $(g_{x,d})_{l,m}$, together with the well-known addition formula of spherical harmonic functions [57]:

$$\sum_{m=-l}^{l} \overline{Y_l^m(\theta_{\widehat{k}}, \phi_{\widehat{k}})} Y_l^m(\theta_\xi, \phi_\xi) = P_l^0(\widehat{k} \cdot \xi)\,, \tag{4.24}$$

whenever $\widehat{k}, \xi \in \mathbb{S}^2$, as well as the following generating function [3] of the Legendre polynomials $P_l := P_l^0$:

$$\frac{1}{\sqrt{r^2 - 2zr + 1}} = \sum_{l=0}^{\infty} r^l P_l(z)\,, \quad \forall z, r \in \mathbb{C}\,, \tag{4.25}$$

we can derive, after some basic calculations, the following explicit expression of the probing function $\eta_{x,d}$:

$$\eta_{x,d}(\xi) = \frac{d \cdot \xi - \frac{(x-\xi)\cdot d}{|x-\xi|}}{\sqrt{4\pi}(|x - \xi| - x \cdot \xi + 1)}\,, \quad \text{for } \xi \in \mathbb{S}^2\,. \tag{4.26}$$

In what follows, we would also like to calculate explicitly the duality product $\langle \cdot, \cdot \rangle_\gamma$ between the probing functions with $\gamma \geq 0$. We note the facts that η_{x,d_x} and η_{y,d_y} are in $H^\gamma(\partial\Omega)$, and that the complete orthonomal set $\{Y_l^m(\theta,\phi)\}_{l\in\mathbb{Z},-m\leq l\leq m}$ in $L^2(\mathbb{S}^2)$ are the eigenfunctions of the surface Laplacian operator $-\Delta_{\mathbb{S}^2}$ with each of their corresponding eigenvalues as $l(l+1)$. Therefore, by the definition of the duality product $\langle \cdot, \cdot \rangle_\gamma$ on $\mathbb{S}^2$ in (2.1) and using the fact that the probing functions have a zero mean over $\mathbb{S}^2$, we obtain the following explicit expression for the duality product $\langle \cdot, \cdot \rangle_{\gamma,\partial\Omega}$ for η_{x,d_x} and η_{y,d_y}:

$$\langle \eta_{x,d_x}, \eta_{y,d_y} \rangle_{\gamma,\mathbb{S}^2} = \sum_{l=1}^{\infty} \sum_{m=-l}^{l} l^\gamma (l+1)^\gamma \overline{(g_{x,d_x})_{l,m}} (g_{y,d_y})_{l,m}. \tag{4.27}$$

Then applying (4.23) and (4.24), we further derive

$$\langle \eta_{x,d_x}, \eta_{y,d_y} \rangle_{\gamma,\mathbb{S}^2} = \left(d_x \cdot \nabla_{k_x} \circ d_y \cdot \nabla_{k_y}\right) \left(\sum_{l=1}^{\infty} l^{\gamma-2} (l+1)^\gamma (r_{k_x} r_{k_y})^l P_l(\widehat{k_x} \cdot \widehat{k_y}) \right) \Big|_{(k_x,k_y)=(x,y)}. \tag{4.28}$$

Using (4.25), the expression (4.28) with $\gamma = 1$ directly reduces to

$$\begin{aligned} \langle \eta_{x,d_x}, \eta_{y,d_y} \rangle_{1,\mathbb{S}^2} \quad = \quad & - \frac{\frac{2x\cdot d_x y\cdot d_y - d_x\cdot d_y}{\sqrt{|x|^2|y|^2-2x\cdot y+1}} - \frac{(|x|^2 y\cdot d_y - x\cdot d_y)(|y|^2 x\cdot d_x - y\cdot d_x)}{(|x|^2|y|^2-2x\cdot y+1)^{\frac{3}{2}}} - d_x\cdot d_y}{\sqrt{|x|^2|y|^2-2x\cdot y+1} - x\cdot y + 1} \\ & + \frac{(\frac{|x|^2 y\cdot d_y - x\cdot d_y}{\sqrt{|x|^2|y|^2-2x\cdot y+1}} - x\cdot d_y)(\frac{|y|^2 x\cdot d_x - y\cdot d_x}{\sqrt{|y|^2|x|^2-2y\cdot x+1}} - y\cdot d_x)}{(\sqrt{|x|^2|y|^2-2x\cdot y+1} - x\cdot y + 1)^2} \\ & + \frac{3(|x|^2 y\cdot d_y - x\cdot d_y)(|y|^2 x\cdot d_x - y\cdot d_x)}{(|x|^2|y|^2-2x\cdot y+1)^{\frac{5}{2}}} - \frac{2(x\cdot d_x)(y\cdot d_y) - d_x\cdot d_y}{(|x|^2|y|^2-2x\cdot y+1)^{\frac{3}{2}}}. \end{aligned} \tag{4.29}$$

On the other hand, for the sake of exposition, we define for the case with $\gamma \geq 2$, $\gamma \in \mathbb{N}$ the following auxiliary function $F^\beta(r,x)$ for $\beta \in \mathbb{N}$, $r > 0$ and $x \in \mathbb{C}$ such that $|x| < 1$,

$$F^\beta(r,x) := \left(r\frac{\partial}{\partial r}\right)^\beta \left(\frac{1}{\sqrt{r^2-2rx+1}}\right) = \sum_{l=0}^{\infty} l^\beta r^l P_l(x), \tag{4.30}$$

where the second equality comes from (4.25). This function can be explicitly calculated for any $\beta \in \mathbb{N}$ in a recursive way. Using this function and (4.28), we directly deduce the following expression of the duality products $\langle \cdot, \cdot \rangle_\gamma$ for $\gamma \geq 2$:

$$\langle \eta_{x,d_x}, \eta_{y,d_y} \rangle_{\gamma,\mathbb{S}^2} = \sum_{m=0}^{\gamma} C_m^\gamma \left(d_x \cdot \nabla_{k_x} \circ d_y \cdot \nabla_{k_y}\right) \left(F^{m+\gamma-2}(r_{k_x} r_{k_y}, \widehat{k_x} \cdot \widehat{k_y})\right) \Big|_{(k_x,k_y)=(x,y)} \tag{4.31}$$

which can bse calculated explicitly with the help of (4.30) up to any order recursively. We again observe that the terms x, y, d_x, d_y in the duality products $\langle \cdot, \cdot \rangle_{\gamma,\partial\Omega}$ are deeply coupled. However, we can see, substituting (4.31)-(4.29) into (2.3), that the kernel (2.3) still attains maximum when x is near y and when $d_x \approx d_y$. We can therefore use the index function to locate inclusions efficiently, and this justifies the validity of the DSM for EIT for the open ball. As an example, we plot the duality product $\langle \cdot, \cdot \rangle_1$ with $x = (r_x, \widehat{x})$, $r_x = 0.4$, $\widehat{x} \in \mathbb{S}^2$, $y = (0.5, 0, 0)$ for different probing directions; see Figure 3. We can see that for the case when $d_x \approx d_y$, it gives a larger value when $x \approx y$ with a sharply peaked Gaussian like distribution. However, for the case when d_x is not approximately equal to d_y, the duality product $\langle \cdot, \cdot \rangle_1$ gives two local extrema when x is near y, and we cannot conclude that it attains maximum when $x \approx y$ with a sharply peaked Gaussian like distribution.

With a similar argument as above, we may also derive an explicit expression of the probing functions and their duality products $\langle \cdot, \cdot \rangle_{\gamma,\partial\Omega}$ on an n-dimensional open ball where $n \in \mathbb{N}$ with the help of the $(n-1)$-th ultraspherical harmonic functions.

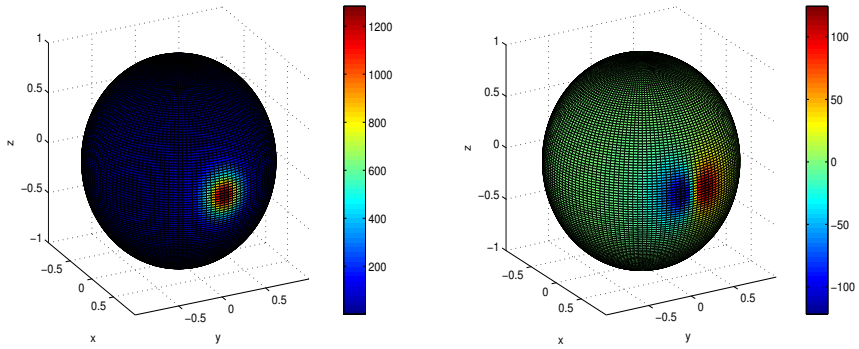

Figure 3: Duality product $\langle \cdot, \cdot \rangle_1$ for $x = (r_x, \widehat{x})$, $r_x = 0.4$, $\widehat{x} \in \mathbb{S}^2$, $y = (0.5, 0, 0)$, when $d_x = d_y = (1, 0, 0)$ (Left) and when $d_x = (1, 0, 0)$, $d_y = (0, 1, 0)$ (Right).

5 Optimal current density

In this section, we shall analyze the sensitivity of the scattered potential field $u - u_0$, where u is the total field satisfying (1.1) and u_0 is the incidence field satisfying the homogeneous system (3.1), with respect to different choice of current density g in (1.1). From such analysis, we can thereby obtain a choice of g which is optimal for the reconstruction of the inhomogeneities D, which we will use in our numerical experiments in the next section. In order to carry out our desired analysis, we first subtract (3.1) from (1.1) to obtain

$$\nabla \cdot (\sigma \nabla (u - u_0) + (\sigma - \sigma_0) \nabla u_0) = 0 \quad \text{in } \Omega\,; \quad \frac{\partial (u - u_0)}{\partial \nu} = 0 \quad \text{on } \partial\Omega\,; \quad \int_{\partial\Omega} (u - u_0)\, ds = 0\,. \tag{5.1}$$

Multiplying both sides of the equation with $u - u_0$, then integrating over Ω and using the fact that $\sigma = \sigma_0$ on $\partial\Omega$, we obtain the following equation

$$\int_\Omega (\sigma |\nabla (u - u_0)|^2 + (\sigma - \sigma_0) \nabla u_0 \cdot \nabla (u - u_0)) dx = 0\,. \tag{5.2}$$

Then it follows from the Cauchy-Schwartz inequality that the following estimate for the energy of $u - u_0$ holds

$$\int_\Omega \sigma |\nabla (u - u_0)|^2\, dx \leq \int_\Omega \frac{(\sigma - \sigma_0)^2}{\sigma} |\nabla u_0|^2\, dx = \int_D \frac{(\sigma - \sigma_0)^2}{\sigma} |\nabla u_0|^2\, dx. \tag{5.3}$$

This estimate is important in the sense that it tells us that the energy of the scattered potential field is controlled by that of the incidence field u_0 inside the inhomogeneities D.

Next, we restrict ourselves to the special domain of spherical geometry, namely $\Omega = B_1(0) \subset \mathbb{R}^2$, and $\partial\Omega = \mathbb{S}^1$, in order to achieve a more explicit and quantitative estimate. In this case, we can write g in (1.1) in the following form

$$g(\theta) = \frac{1}{\sqrt{2\pi}} \sum_{m \in \mathbb{Z}\backslash\{0\}} [\mathfrak{F}(g)](m) e^{im\theta}\,, \quad \theta \in (0, 2\pi)\,, \tag{5.4}$$

where $[\mathfrak{F}(g)](m)$ are the Fourier coefficients of g defined as in (4.9) for all $m \in \mathbb{Z}\backslash\{0\}$. Then we can see that the solution u_0 to (3.1) can be expressed as

$$u_0(x) = \sum_{m \in \mathbb{Z}\backslash\{0\}} [\mathfrak{F}(g)](m) u_m(x)\,, \quad x \in \Omega\,, \tag{5.5}$$

where u_m is defined by (4.4). We hope to calculate explicitly the term at the right hand side of the inequality (5.3). By direct computings, we obtain that

$$\frac{\partial u_m}{\partial x_1} = (x_1 - ix_2\mathrm{sgn}(m))\, r^{|m|-2}e^{im\theta}, \quad \frac{\partial u_m}{\partial x_2} = (x_2 + ix_1\mathrm{sgn}(m))\, r^{|m|-2}e^{im\theta}. \tag{5.6}$$

For convenience, we shall often write below that for $m \in \mathbb{Z}\backslash\{0\}$ and $z \in \mathbb{C}$, $f(z,m) = z$ if $m > 0$ and $f(z,m) = \overline{z}$ if $m < 0$, and

$$C(\theta, m, l) = f(e^{i\theta}, l)f(e^{-i\theta}, m) + f(-ie^{i\theta}, l)f(ie^{-i\theta}, m) \tag{5.7}$$

for $\theta \in (0, 2\pi)$ and $l, m \in \mathbb{Z}\backslash\{0\}$. We notice that $C(\theta, m, l)$ is at most of modulus 2 with $C(\theta, m, m) = 2$. Combining (5.6) with the above expressions, we have for all $l, m \in \mathbb{Z}\backslash\{0\}$ that

$$\int_D \frac{(\sigma - \sigma_0)^2}{\sigma}\overline{\nabla u_l} \cdot \nabla u_m \, dx = \int_D C(\theta, m, l)e^{i(m-l)\theta}r^{|m|+|l|-2}\frac{(\sigma(x) - \sigma_0)^2}{\sigma(x)}\, dx \tag{5.8}$$

where $x = (r, \theta)$ is in its polar coordinate. Therefore, given $N \in \mathbb{N}$, if the current g in (1.1) is such that $[\mathfrak{F}(g)](m) = 0$ for $|m| < N$, we obtain from the estimates above that

$$\begin{aligned} \int_\Omega \sigma|\nabla(u - u_0)|^2\, dx &\leq \int_D \frac{(\sigma - \sigma_0)^2}{\sigma}|\nabla u_0|^2\, dx \\ &= 2\int_D \frac{(\sigma - \sigma_0)^2}{\sigma}\left((|[\mathfrak{F}(g)](N)|^2 + |[\mathfrak{F}(g)](-N)|^2)r^{2N-2} + O(r^{2N-1})\right) dx. \end{aligned} \tag{5.9}$$

Therefore the Fourier modes $[\mathfrak{F}(g)](m)e^{im\theta}$ with $|m| = N$ in g dominate in (5.9), whereas the effects of higher frequency components decrease rapidly since $r < 1$ in $B_1(0)$. It means that currents of the form $g = e^{im\theta}$ where $m \in \mathbb{Z}\backslash\{0\}$ are the optimal currents that maximize the sensitivity of the scattered potential $u - u_0$. Therefore, choosing currents of such a form shall give the best scattered potential for the reconstruction of the inhomogeneities D inside Ω for the EIT problem.

6 Numerical experiments

In this section we shall present some numerical examples to demonstrate the efficiency and accuracy of the newly proposed DSM for the reconstruction of inhomogeneous inclusions in the EIT problem.

In the following 4 examples, we first consider the sampling region $\Omega = [-1, 1]^2$ as a square domain with the homogeneous background conductivity being $\sigma_0 = 1$. In each of the 4 examples, there are some inhomogeneous inclusions inside the sampling domain, with their conductivity always set to be $\sigma = 5$. In order to generate the observed data of the forward problem, we solve (1.1) by second order centered finite difference scheme with a fine mesh size $h = 1/100$ and the current g being of the form $g = \cos(2\pi kx)$ where $k \in \mathbb{N}$ is to be chosen. This choice of g maximizes the sensitivity for reconstructing the inclusions (see section 5 for a detailed explanation). When the domain Ω is a square, we have to map the cosine function to the four boundaries of the square domain. This is performed via a composition $\cos \circ m_{2\pi} \circ \phi^{-1}$ of the cosine function with the inverse of a parametrization ϕ on the boundary, where ϕ is the mapping that maps the interval $[0, 1]$ onto the boundary with unit speed in the clockwise direction and $m_{2\pi}$ stands for the multiplication by 2π. We would like to emphasize that, in each of our numerical experiments, only one incident current is made to generate the observed data, therefore we have only a single pair of Cauchy data available in our numerical reconstruction. In addition, we introduce some random noise in the scattered potential field $u_s := \Lambda_\sigma g - \Lambda_{\sigma_0} g$ pointwisely in the form:

$$u_s^\delta(x) = u_s(x) + \varepsilon\delta|u_s(x)| \tag{6.1}$$

where δ is uniformly distruted between $[-1, 1]$ and ε refers to the relative noise level. In the following 4 examples, we always set the noise level to be $\varepsilon = 5\%$.

We then use the new DSM introduced in section 2.3 to recover the location of inhomogeneities D from the noisy observed data u_s^δ by calculating the index function $I(x, d_x)$ defined as in (2.15), where the integration over $\partial\Omega$ is performed by the rectangular quadrature rule with mesh size $1/90$. From our numerical experiments, we observe that the squared index $(I(x, d_x))^2$ gives us sharper images of the inclusions, hence providing a more accurate estimate of the support of the inhomogeneities D. Therefore, in each of the following examples, we provide both the reconstructed images from the index function I and the squared index I^2. In all our experiments, we always choose the probing direction $d_x = \frac{\nabla\phi(x)}{|\nabla\phi(x)|}$ at each point $x \in \Omega$ where ϕ is defined as in (2.18) (see section 2.4 for further explanation).

Example 1. In this example, the medium consists of 2 inclusions of size 0.1×0.1 centered at $(-0.44, -0.44)$ and $(0.36, 0.36)$ respectively; see Figure 4 (left). The current g is chosen to be $g = \cos(2\pi x)$. Figure 4 (middle and right) show the respective reconstructed images from the index function I and the squared index I^2. From the figures, we can see that both scatterers are well separated, and their locations are recovered pretty satisfactorily, considering that only a single pair of Cauchy data is used.

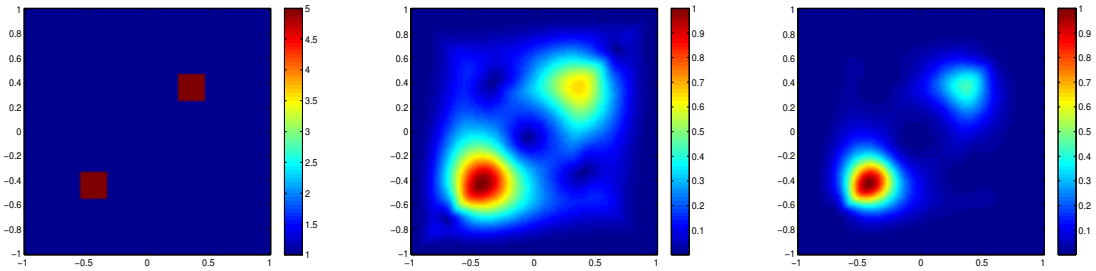

Figure 4: Exact medium image of Example 1 (left); reconstructed images by index function I (middle) and the squared index I^2(right).

Example 2. This example tests a medium with 2 inclusions sitting on the same row horizontally, located respectively at the positions $(-0.47, 0.38)$ and $(0.38, 0.38)$; see Figure 5 (left). The size of the inclusions and the current g are of the same as in Example 1. The reconstructed images are shown in Figure 5 (middle and right). From the figure, we observe now that the scatterers are closer to each other and there are coupling effect between them such that they tend to merge. However, the locations of both scatterers are still recognisable, and the reconstruction is pretty satisfactory, considering that only a single pair of Cauchy data is used.

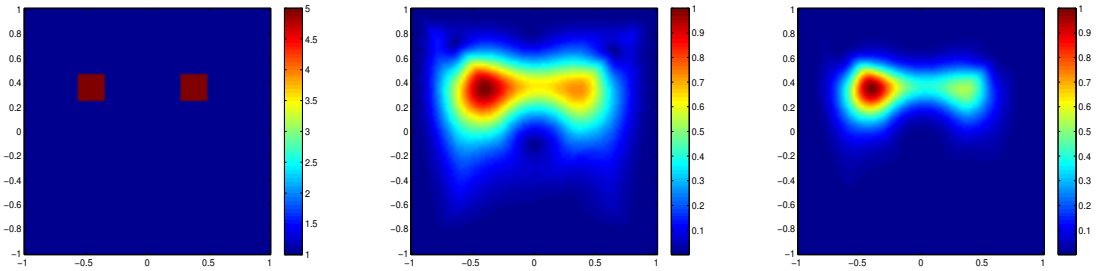

Figure 5: Exact medium image of Example 2 (left); reconstructed images by index function I (middle) and the squared index I^2(right).

Example 3. 4 inclusions are considered in this example; see Figure 6 (left), with the current and each inclusion being the same size as the one in Example 1. The respective positions of the scatterers are $(-0.51, -0.51)$ $(0.44, 0.44)$, $(-0.58, 0.38)$ and $(0.38, -0.58)$. Figure 6 (middle and right) show the reconstructed images. We can clearly observe a close coupling effect among all the scatterers, and the scatterers shift towards inward. But considering the severe ill-posedness of the EIT problem and the fact that only a single pair of Cauchy data is used, we think the numerical reconstruction is quite satisfactory

under a 5% noise in the data, as the 4 scatterers are well separated and located also reasonably well.

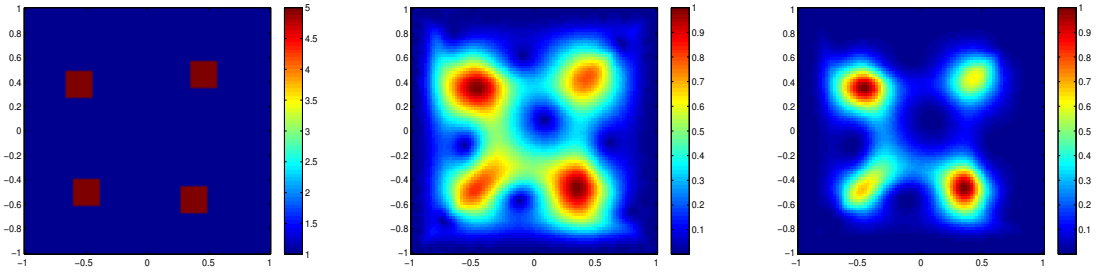

Figure 6: Exact medium image of Example 3 (left); reconstructed images by index function I (middle) and the squared index I^2(right).

Example 4. In this example we investigate a medium case with an inclusion of a rectangular annulus of width 0.05 and length 0.28 of the inner square centered at $(0.02, 0.02)$; see Figure 7 (left). We choose the current density g to be $g = \cos(4\pi x)$. Figure 7 (middle and right) show the reconstructed images. This is a difficult example for numerical reconstruction as there is a hole inside the inclusion and the annulus has a very small width. However, considering the severe ill-posedness of the problem and the 5% noise present in the observed data, our reconstruction appears to be quite satisfactory. We can clearly see the hole inside the reconstructed annulus, and both the location and the shape of the scatterer are accurately reconstructed.

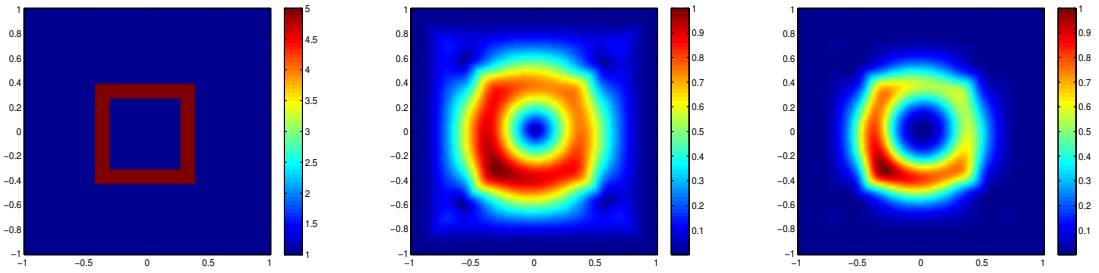

Figure 7: Exact medium image of Example 4 (left); reconstructed images by index function I (middle) and the squared index I^2(right).

In the remainder of this section, we shall consider another widely used sampling domain in applications, the circular domain $\Omega = B_1(0) \subset \mathbb{R}^2$. Again, in each of the following examples, there are some inhomogeneous inclusions with conductivity $\sigma = 5$ inside the sampling domain, whereas the homogeneous background conductivity is always set to be $\sigma_0 = 1$. Noisy data is generated according to (6.1) with ε always set to be $\varepsilon = 3\%$. In all our tests, we take the incident current g to be $g = \cos(2\pi\theta)$. The reconstruction process from the index function is similar to the previous examples except that the integration over $\partial\Omega = \mathbb{S}^1$ is now performed by the rectangular quadrature rule with mesh size $\pi/64$. Same as in the previous examples, we always choose the probing direction $d_x = \frac{\nabla\phi(x)}{|\nabla\phi(x)|}$ for $x \in \Omega$ where ϕ is defined as in (2.18) when we calculate our reconstructed images based on the index function $I(x, d_x)$ in (2.15) and the squared index $(I(x, d_x))^2$.

Example 5. In this example, we consider the case with 2 inclusions of size 0.1×0.1 respectively at the positions $(-0.44, 0.36)$ and $(0.36, -0.44)$; see Figure 8 (left). Reconstructed images are shown on Figure 8 (middle and right). From the figure, we can see that the scatterers are located quite well, although the coupling effect is now more apparent when we compare with the case of the sampling domain being a square, and that the location of the inclusions are a bit scattered.

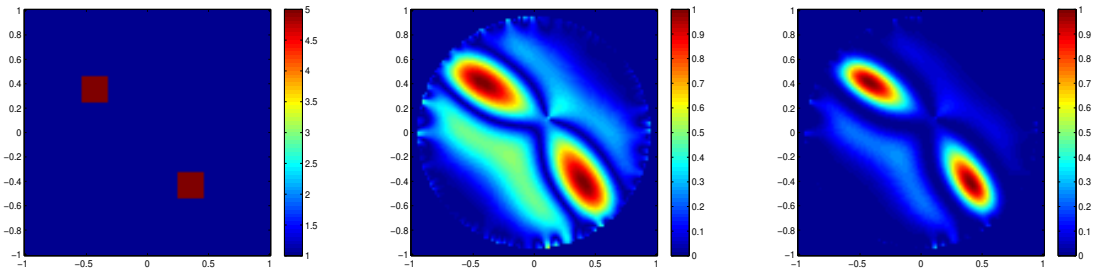

Figure 8: Exact medium image of Example 5 (left); reconstructed images by index function I (middle) and the squared index I^2(right).

Example 6. In this example, 2 inclusions of the same size as in Example 5 are respectively placed at the positions $(-0.36, 0.36)$ and $(0.36, 0.36)$ inside the domain; see Figure 9 (left). The reconstructed images are shown in Figure 9 (middle and right). From the figure, we notice that even the inclusions are put very close to each other, the positions of the scatterers are recovered very well with no obvious coupling effect, although they are now a bit shifted.

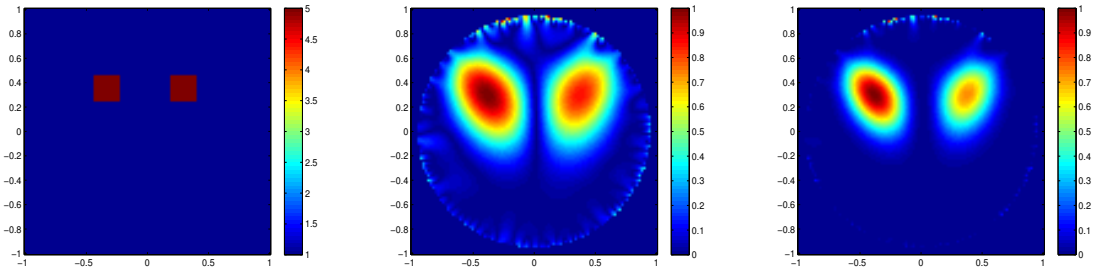

Figure 9: Exact medium image of Example 6 (left); reconstructed images by index function I (middle) and the squared index I^2(right).

Example 7. We now investigate an example with 4 inclusions inside the sampling region, which are placed at positions of $(0.36, 0.36)$, $(0.36, -0.44)$, $(-0.44, 0.36)$ and $(-0.44, -0.44)$ with same size as in Example 5; see Figure 10 (left). The reconstructed images are shown on Figure 10 (middle and right). We can see that there are strong coupling effects among all the scatterers. However, the locations of the scatterers are still recovered with a reasonable accuracy.

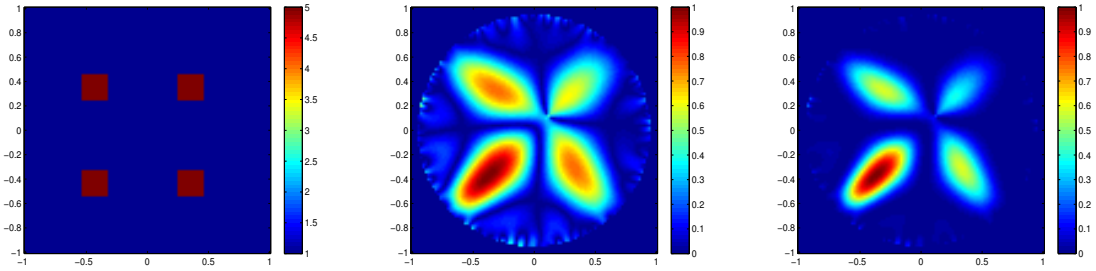

Figure 10: Exact medium image of Example 7 (left); reconstructed images by index function I (middle) and the squared index I^2(right).

We can observe from Examples 5-8 that the reconstructions with the circular sampling domain is not that good as those for the rectangular domain. This may be caused by the extreme symmetry of the circular domain. However, considering the severe ill-posedness of the EIT problem and the fact that only

a single pair of noisy Cauchy data is used, the numerical reconstructions are quite satisfactory with the newly proposed simple direct sampling method.

Acknowledgements

The authors would like to thank two anonymous referees for their many insightful and constructive comments and suggestions, which have helped us improve the organisation and quality of the paper essentially.

References

[1] H. Ammari and H. Kang, Polarization and Moment Tensors: with Applications to Inverse Problems and Effective Medium Theory, Applied Mathematical Sciences Series, Volume 162, Springer-Verlag, New York, 2007.

[2] H. Ammari and H. Kang, Reconstruction of Small Inhomogeneities from Boundary Measurements, Lecture Notes in Mathematics, Volume 1846, Springer-Verlag, Berlin 2004.

[3] G.B. Arfken and H.J. Weber, Mathematical Methods for Physicists, Elsevier Academic Press (2005).

[4] A. E. Badia and T. Ha-Duong, An inverse source problem in potential analysis, Inverse Problems, 16(3) (2000), pp. 651-663.

[5] D.C. Barber and B.H. Brown, Applied potential tomography, J. Phys. E: Sci. Instrum., 17 (1984), pp. 723-733.

[6] R.H. Bayford, Bioimpedance tomography (electrical impedance tomography), Ann. Rev. Biomed.Eng.,8 (2006), pp. 63-91.

[7] C. Bellis, A. Constantinescu, T. Coquet,T. Jaravel and A. Lechleiter, A non-iterative sampling approach using noise subspace projection for EIT, Inverse Problems (2012), DIO:10.1088/0266-5611/28/7/075015.

[8] M. Bonnet, Higher-order topological sensitivity for 2-D potential problems, application to fast identification of inclusions, Int. J. Solids Struct., 46 (11-12), (2009), pp. 2275-2292.

[9] L. Borcea, Electrical impedance tomography, Inverse Problems, 18 (2002), R99-136.

[10] A. Borsic, B.M. Graham, A. Adler and W.R.B. Lionheart, In vivo impedance imaging with total variation regularization, IEEE Trans. Med. Imaging, 29 (2010), pp. 44-54.

[11] M. Brühl, Explicit characterization of inclusions in electrical impedance tomography, SIAM J. Math. Anal., 32 (2001), pp. 1327-1341.

[12] M. Brühl and M. Hanke, Numerical implementation of two noniterative methods for locating inclusions by impedance tomography, Inverse Problems, 16 (2000), pp. 1029-1042.

[13] M. Brüh and M. Hanke, Recent progress in electrical impedance tomography, Inverse Problems, 19 (2003), S65-S90.

[14] M. Brühl, M. Hanke and M. Pidcock, Crack detection using electostatic measurements, ESAIM: Mathematical Modelling and Numerical Analysis, 35 (3), (2001), pp. 595-605.

[15] A.P. Calderón, On an inverse boundary value problem, Seminar on Numerical Analysis and its Applications to Continuum Physics (Rio de Janeiro, 1980), Soc. Brasil. Mat., Rio de Janeiro (1980), pp. 65-73.

[16] D.J. Cedio-Fengya, S. Moskow, M. S. Vogelius, Identication of conductivity imperpections of small diameter by boundary measurements: Continuous dependence and computational reconstruction, Inverse Problems 14 (1998), pp. 553595.

[17] M. Cheney, D, Isaacson, J.C. Newell, S. Simske and J. Goble, NOSER: an algorithm for solving the inverse conductivity problem, Int. J. Imaging Syst. Technol., 2(1990), pp. 66-75.

[18] K-S. Cheng, D. Isaacson, J.C. Newell and D.G. Gisser, Electrode models for electric current computed tomography, IEEE Trans. Biomed. Eng., 36(1989), pp. 918-924.

[19] E.T. Chung, T.F. Chan and X-C. Tai, Electrical impedance tomography using level set representation and total variational regularization, J. Comput. Phys., 205 (2005), pp. 357-372.

[20] A. J. Devaney, Time reversal imaging of obscured targets from multistatic data. IEEE Trans. Antennas Propag., 53, pp. 1600-1610, 2005.

[21] D.C. Dobson and F. Santosa, An image-enhancement technique for electrical impedance tomography, Inverse Problems, 10 (1994), pp. 317-334.

[22] K. Erhard and R. Potthast, The point source method for reconstructing an inclusion from boundary measurements in electrical impedance tomography and acoustic scattering, Inverse Problems 19(5), (2003), 1139.

[23] M. Gehre, T. Kluth, A. Lipponen, B. Jin, P. Maass, A. Seppanen and J.P. Kaipio, Sparsity reconstruction in electrical impedance tomography: an experimental evaluation, J. Comput. Appl. Math, 236 (2012), pp. 2126-2136.

[24] L. Göcke, S. Rust, U. Weihs, T. Günther and C. Rücker, Combining sonic and electrical impedance tomography for the nondestructive testing of trees Western Arborist, Berlin: Springer (2008), pp. 1-11.

[25] D.J. Griffiths, Introduction to Electrodynamics (3rd ed.). Prentice Hall (1999).

[26] M. Hanke and B. Schappel, The factorization method for electrical impedance tomography in the half-space, SIAM J. Appl. Math., 68 (2008), pp. 907-924.

[27] C. Hähnlein, K. Schilcher, C. Sebu and H. Spiesberger, Conductivity imaging with interior potential measurements, Inverse Problems Sci. Eng., 19(2011), pp.729-750.

[28] D. Holder, Electrical Impedance Tomography, Institute of Physics Publishing, Bristol and Philadelphia (2005).

[29] D. Holder, D. Isaacson, J. Müller and S. Siltanen, editors, Physiol. Meas., 25 (2003), no 1.

[30] M. Ikehata, Reconstruction of inclusion from boundary measurements, J. Inv. Ill-Posed Problems, 10 (2002) pp. 37-65, 2002.

[31] D. Isaacson, J.C. Newell, J.C. Goble, and M. Cheney, Thoracic impedance images during ventilation, Annual Conference of the IEEE Engineering in Medicine and Biology Society, 12,(1990), pp. 106-107.

[32] K. Ito, B. Jin and J. Zou, A direct sampling method to inverse medium scattering problem, Inverse Problems, 28(2) (2012), 025003.

[33] B. Jin and P. Maass, Sparsity regularization for parameter identification problems, Inverse Problems, 28 (2012), 123001.

[34] B. Jin, T. Khan and P. Maass, A reconstruction algorithm for electrical impedance tomography based on sparsity regularization, Int. J. Numer. Methods Eng., 89 (2012), pp. 337-353.

[35] B. Jin, T. Khan, P. Maass and M. Pidcock, Function spaces and optimal currents in impedance tomography, J. Inverse Ill-Posed Problems, 19 (2011), pp. 25-48.

[36] B. Jin and P. Maass, An analysis of electrical impedance tomography with applications to Tikhonov regularization, ESAIM: Control Optim. Calc. Var., 18 (2012), pp. 1027-1048.

[37] J. Jordana, J.M. Gasulla and R. Paolas-Areny, Electrical resistance tomography to detect leaks from buried pipes, Meas. Sci. Technol., 12(2001), pp. 1061-1068.

[38] J. Jossinet, The impedivity of freshly excised human breast tissue, Physiol. Meas., 19(1998), pp. 61-75.

[39] J. Kaipio, V. Kolehmainen V, M. Vauhkonen and E. Somersalo, Inverse problems with structural prior information, Inverse Problems, 15(1999), pp. 713-729.

[40] J. Kaipio and E. Somersalo, Statistical and Computational Inverse Problems, New York: Springer (2005).

[41] J.P. Kaipio, V. Kolehmainen, E. Somersalo and M. Vauhkonen, Statistical inversion and Monte Carlo sampling methods in electrical impedance tomography, Inverse Problems, 16(2000), pp. 1487-1522.

[42] A. Kirsch and N. Grinberg, The Factorization Method for Inverse Problems, Oxford: Oxford University Press (2008).

[43] T. Kolokolnikov and A.E. Lindsay, Recovering multiple small inclusions in a three-dimensional domain using a single measurement Inverse Problems in Science and Engineering, 1 (2014), DOI: 10.1080/17415977.2014.906414 .

[44] J. Li and J. Zou, A direct sampling method for inverse scattering using far-field data, Inverse Problems and Imaging, 7 (2013), 757-775.

[45] W.R.B. Lionheart, EIT reconstruction algorithms: pitfalls, challenges and recent developments, Phys. Meas., 25(2004), pp.125-142.

[46] M. Lukaschewitsch, P. Maass and M. Pidcock, Tikhonov regularization for electrical impedance tomography on unbounded domains, Inverse Problems, 19(2003), pp.585-610.

[47] T. Martin and J. Idier, A FEM-based nonlinear MAP estimator in electrical impedance tomography, ICIP: Proc. IEEE Int. Conf. on Image Processing, 2(1997), pp. 684-687.

[48] M.K. Pidcock, M. Kuzuoglu and K. Leblebicioglu, Analytic and semi-analytic solutions in electrical impedance tomography. I. Two-dimensional problems, Physiol. Meas., 16 (1995) pp. 77-90.

[49] R. Potthast, A study on orthogonality sampling, Inverse Problems, 26 (2010), 074015 (17pp).

[50] L. Rondi, On the regularization of the inverse conductivity problem with discontinuous conductivities, Inverse Problems and Imaging, 2(2008), pp. 397-409.

[51] L. Rondi, F. Santosa, Enhanced electrical impedance tomography via the MumfordShah functional, ESAIM: Control Optim. Calc. Var., 6(2001), pp. 517-538.

[52] S. Siltanen, J. Mueller and D. Isaacson, An implementation of the reconstruction algorithm of A Nachman for the 2D inverse conductivity problem, Inverse Problems, 16(2000), pp.681-99.

[53] P.C. Sabatier and C. Sebu C, On the resolving power of electrical impedance tomography, Inverse Problems, 23 (2007), pp. 1895-1913.

[54] T. Sjödén and S. Nordebo, Sensitivity analysis for measurement configuration evaluation in electrical impedance tomography, Inverse Problems Sci. Eng. (2012), submitted.

[55] G. Uhlmann, Electrical impedance tomography and Calderón's problem, Inverse Problems, 25 (2009), 123011.

[56] P. Vauhkonen, M. Vauhkonen, T. Savolainen and J. Kaipio, Three-dimensional electrical impedance tomography based on the complete electrode model, IEEE Trans. Biomed. Eng., 46(1999), pp.1150-1160.

[57] G.N. Watson and E.T. Whittaker, A Course of Modern Analysis, Cambridge University Press (1927).

[58] T.J. Yorkey, J.G. Webster and W.J. Tompkins, Comparing reconstruction algorithms for electrical impedance tomography, IEEE Trans. Biomed. Eng., 34(1987), pp.843-852.

[59] M.S. Zhdanov and G.V. Keller, The geoelectrical methods in geophysical exploration, Methods in Geochemistry and Geophysics, 31, Elsevier (1994).

[60] Y. Zou and Z. Guo, A review of electrical impedance techniques for breast cancer detection, Med. Eng. Phys., 25(2003), pp. 79-90.